Surface Science 757 (2025) 122740

Contents lists available at ScienceDirect

Surface Science

journal homepage: www.elsevier.com/locate/susc

Modeling the self-assembly of L-cysteine molecules on the Au(111) surface: A lattice model approach

Mary Tabut [a,b], Pavel V. Stishenko [c], Monica Calatayud [b,*]

[a] Sorbonne Université, CNRS, Laboratoire de Chimie Théorique, LCT, 4 Place Jussieu F-75005 Paris, France
[b] Sorbonne Université, CNRS, MONARIS, CNRS-UMR 8233, 4 Place Jussieu F-75005 Paris, France
[c] Cardiff Catalysis Institute, School of Chemistry, Cardiff University, Cardiff, United Kingdom

ARTICLE INFO

Keywords:
DFT
SAMS
Chirality
Automatized sampling

ABSTRACT

The design of chiral materials with enhanced properties has rapidly gained interest. However, the complex modeling of self-assembled monolayers poses significant challenges to theoretical chemists, making it difficult to accurately predict or explain the structure and thermodynamic properties of adsorption layers in surface science. In the present work, we provide new insights into the self-assembly network of L-cysteine molecules on an Au (111) surface using a lattice model approach. The research focuses on the adsorption behavior of L-cysteine in its deprotonated acidic form [$NH_3^+CH(CH_2S^-)COOH$)], which introduces unique intermolecular interactions due to the charged amino group. Using the Surface Science Modeling and Simulation Toolkit (SuSMoST), we systematically explored multiple adsorption sites and configurations, generating unexplored high-coverage systems that were further analyzed at the density functional level of theory. Our findings highlight the significance of surface arrangements, intra- and inter-molecular interactions in determining the overall stability of the L-cysteine self-assembled monolayers. Among the various configurations analyzed, a newly identified system revealed the highest stability with an adsorption energy of -1.44 eV, competing with previously reported structures.

1. Introduction

Self-assembled monolayers (SAMs) play a crucial role in surface science and nanotechnology [1–3]. These ordered molecular assemblies form spontaneously when surfactant molecules adsorb onto a substrate, creating highly organized structures that can be adjusted for specific applications [4,5]. One particularly exciting feature of SAMs is their ability to introduce chirality at the nanoscale, which can significantly enhance the optical [6], electronic [7,8], and catalytic properties [9] of the substrate. The unique properties imparted by chirality on nanoparticles (NPs) can be harnessed to unlock new technological opportunities. As a result, researchers have intensely focused on synthesizing, characterizing, and understanding chiral materials, to effectively control and manipulate this property [10,11]. By arranging molecules in specific patterns, SAMs can introduce new properties that are not present in isolated molecules or bare nanoparticle surfaces. For instance, the collective organization of chiral molecules in SAMs can induce surface plasmon resonance (SPR) with unique chiral optical responses, which is crucial for advanced applications in biosensing and photonics [12].

To effectively study and characterize SAMs, both experimental and theoretical approaches are necessary. Experimentally, techniques such as scanning tunneling microscopy (STM), atomic force microscopy (AFM), X-ray photoelectron spectroscopy (XPS) etc.… are invaluable for probing the structure and composition of SAMs. These methods provide critical data that can validate and refine theoretical models. In contrast, theoretical models are essential to predict new structural arrangements and understand the interactions at play in SAMs, guide experimental efforts, and offer insights that may not be directly observable [13,14].

However, modeling these molecular assemblies presents a substantial challenge for theoretical chemists. The complexity arises from the need to accurately predict the interactions and spatial arrangements of molecules on a surface, considering factors such as Van der Waals forces, hydrogen bonding, and steric effects. The number of possible configurations is vast and highly dependent on the type of molecule involved, making manual exploration a hard challenge. Hence, sophisticated computational techniques and robust theoretical models are required to capture these nuances. To date, programs such as metadynamics or ab initio random structure search (AIRSS) are available to automatically sample surface arrangements [15–17]. In this work, we utilized the Surface Science Modeling and Simulation Toolkit (SuSMoST) to

* Corresponding author.
E-mail address: monica.calatayud@sorbonne-universite.fr (M. Calatayud).

https://doi.org/10.1016/j.susc.2025.122740
Received 19 December 2024; Received in revised form 20 February 2025; Accepted 18 March 2025
Available online 20 March 2025

systematically explore the chemical arrangement of l-cysteine on the gold (111) surface, a system that has already received extensive attention both experimentally and theoretically [18–20].

While most theoretical studies have focused on the cysteine molecule in its neutral [$NH_2CH(CH_2SH)COOH$] or zwitterionic form [$NH_3^+CH(CH_2SH)COO^-$] [20–22], our research explores the adsorption behavior of cysteine in an alternative form that can be found under acidic conditions: [$NH_3^+CH(CH_2SH)COOH$]. It is well-established that cysteine adsorbs onto gold surfaces primarily via its sulfur atom. Depending on the medium, this adsorption can occur through the sulfur in its protonated thiol (-SH) or in a deprotonated thiolate form (-S^-). The deprotonated thiolate is often observed in studies involving neutral or slightly basic conditions, where the cysteine molecule undergoes SH bond dissociation. Under acidic conditions, the cysteine molecule has a protonated amino group (NH_3^+) and a neutral carboxyl group (COOH). Experimentally, in this acidic form, cysteine has also been observed to undergo deprotonation of the thiol group before adsorption to the gold surface [23,24] and to exhibit intermolecular interactions between its positively charged amino group and the carboxylic one [25]. Previous theoretical work [22] showed that at low coverage on the Au(111) surface, the deprotonated acidic form is found to be more stable than the neutral or the zwitterionic. Based on these findings, our study focuses on the [$NH_3^+CH(CH_2S^-)COOH$] molecule to investigate its behavior under high-coverage conditions. In contrast to previous studies, which focused solely on the most stable adsorption site at low coverage to model high coverage [22], our work explores various combinations of adsorption sites to construct high-coverage systems and identify new stable arrangements. To that end, we used the SuSMoST toolkit [26] to automate the sampling process and the construction of high-coverage adsorption structures considering symmetries of the adsorbing surface and adsorption complexes. Using this methodology, we efficiently identified the only previously reported high-coverage structure among the various configurations explored [22]. With the numerous configurations found, we performed density functional theory (DFT) optimizations to compute adsorption and interaction energies, as well as Bader charges. Our results emphasize the significance of surface arrangement and intermolecular interactions in determining the overall stability of these systems, unveiling a novel and stable SAM organization. Notably, we observed that, at high ligand coverage, the system is stable but can also rearrange into a known zwitterionic form of the molecule [$NH_3^+CH(CH_2SH)COO^-$]. In this state, the emergence of intra-molecular interactions further enhances the stability. Additionally, our investigation of various surface arrangements reveals a complex relationship between interaction strengths and stability, suggesting that more stable SAMs may paradoxically exhibit weaker interactions with the underlying surface.

2. Computational details

All calculations were performed at the density functional level of theory (DFT) using the Vienna Ab initio Simulation Package (VASP 6.4.0) [27,28]. Valence electrons of Au, S, H, C, O, and N atoms, corresponding to 11, 6, 1, 4, 6, and 5 valence electrons, respectively, were described using a plane- wave basis set with a cutoff of 450 eV [29]. Core electrons were treated using projector-augmented wave (PAW) pseudopotentials [30] and the PBE exchange-correlation functional [31] was employed with Van der Waals corrections introduced via the Grimme D3 approach [32,33]. To simulate the Au(111) surface, periodic boundary conditions were applied, with a thickness of four atomic layers. The choice of four atomic layers ensures that the slab is thick enough to accurately represent both surface and bulk properties. During DFT optimization, the bottom two layers were fixed to mimic the bulk, while the top two Au layers were fully relaxed. A dipole correction was applied along the z-axis, and a 15°A vacuum region was maintained between the slabs. The Au facet was described as p(4 × 4) slabs, and the Brillouin zone was sampled using a 3 × 3 × 1 k-point mesh generated via the Monkhorst-Pack method [34]. Finally, we used a convergence criterion of 10^{-6} eV for each self-consistent field calculation.

In addition, we conducted a Bader charge analysis [35–37] for all configurations, focusing on the complete system, the empty slab, and the overlayer, with particular attention to the sulfur atoms bonded to the gold surface. We also performed a charge transfer analysis between the organic overlayer and the metallic surface. The calculated values are reported in Table 1.

3. Model

As described in the introduction, our model features the deprotonated acidic L-cysteine molecule adsorbed on a gold (111) surface in the form [$NH_3^+CH(CH_2S^-)COOH$]. In a p(4 × 4) supercell, we define a low-coverage system as a monolayer arrangement containing one l-cysteine molecule per cell. In this configuration, the distance between periodic images of the adsorbed l-cysteine molecules is large enough to consider lateral interactions as negligible. High-coverage structures are accounted for by a monolayer arrangement with two l-cysteine molecules per cell interacting with each other.

Fig. 1 illustrates the general methodology employed in this study. To generate pairs of adsorption complexes, defined as high-coverage systems, we first focused on identifying the optimal adsorption sites for the cysteine molecule at low coverage. In this initial phase, we characterized low-coverage systems as individual adsorption complexes, allowing us to identify the most favorable positions for l-cysteine on the gold (111) surface without any interactions between molecules. Having established these optimal low-coverage configurations, we then used them as the foundation for generating high- coverage systems using one of the various functions available in SuSMoST libraries. By pairing the identified adsorption complexes, we were able to investigate how interactions between multiple l- cysteine molecules influence the overall stability and properties of the adsorbed systems. This pairwise model representation effectively captures adsorption systems comprising any number of complexes with various symmetries, taking into account both long-range and directed lateral interactions between pairs of entities. Finally, we conducted analyses at the density functional theory (DFT)

Table 1
Adsorption and interaction energies, and Bader charges for all systems considered. All energies are given in eV and all charges in |e|.

Final (Initial) Arrangement	E_{ads}	E_{adh}	E_{int}	Bader Charges (qS_1/qS_2)	$q_{Overlayer}$
TB1 (TB)	−1.238	−4.245	−0.976	−0.367 / −0.204	0.649
TB2 (TB)	−1.220	−4.044	−0.601	−0.270 / −0.294	0.614
TB3 (TB)	−1.145	−3.219	−0.552	−0.360 / −0.329	0.542
TB4 (TB)	−1.259	−3.315	−0.761	−0.258 / −0.409	0.559
TB5 (TB)	−1.416	−3.552	−1.636	0.032 / −0.249	0.492
TB6 (BB)	−1.416	−3.570	−1.628	−0.247 / 0.006	0.493
TB7 (BB)	−1.443	−3.565	−1.527	−0.258 / −0.052	0.507
TB8 (BB)	−1.227	−3.967	−0.576	−0.305 / −0.259	0.605
BB1 (BB)	−1.213	−3.522	−0.602	−0.374 / −0.222	0.643
TT1 (TT)	−1.413	−3.344	−1.510	−0.315 / 0.015	0.418
TT2 (TT)	−1.436	−2.905	−1.830	−0.102 /−0.101	0.363
TT3 (TB)	−1.342	−3.555	−0.981	−0.247 /−0.399	0.534
TT4 (TB)	−1.214	−3.524	−0.747	−0.364 /−0.340	0.564
TT5 (TB)	−1.369	−3.042	−1.442	0.045 / −0.338	0.393
TT6 (TB)	−1.296	−3.386	−0.906	−0.379 / −0.237	0.519
TT7 (BB)	−0.904	−4.412	0.139	−0.291 / −0.294	0.643

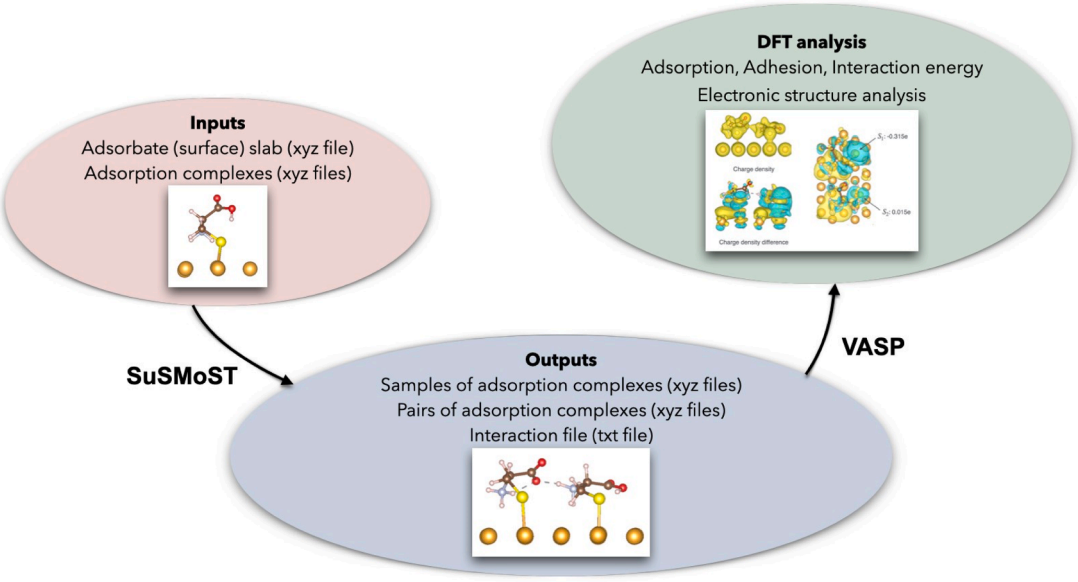

Fig. 1. Scheme representing the methodology followed during this study.

level to further evaluate their properties.

At low-coverage, we explored four adsorption sites available on a gold (111) surface (top, bridge, hollow fcc and hollow hcp). When considering the deprotonated acidic form of the l-cysteine, only the bridge and top positions are found to be stable and not subject to structural reorganization after relaxation. Interestingly, our calculations revealed a close adsorption energy between the bridge and the top site, with only 0.05 eV in favor of the bridge site. With the energy difference being minimal, we considered both possibilities when constructing high-coverage systems. The comparison of these data with previous work is challenging as this specific zwitterionic form of the molecule did not receive much attention. The only direct study of this specific molecular state of cysteine is from Morales et al. [22], who identified the top site as the most stable adsorption site. Our findings differ from them, as they did not report the bridge site as a possible arrangement. Interestingly, other studies focusing on different states of cysteine support the bridge site as the most stable. For example, Gharabekyan et al. [38] found the bridge site most stable for protonated cysteine, while Fajín et al. [20] reported similar results for neutral and zwitterionic forms. Although these studies do not investigate the exact molecular state of cysteine we are considering, they support the stability of the bridge site.

Fig. 2 illustrates the different adsorption complexes used in the SuSMoST program to generate high- coverage systems. Since the toolkit operates using symmetries, we accounted for two types of bridge sites. While these periodic configurations show nearly identical adsorption energies, we observed that focusing on only one of them would overlook configurations such as the bridge/bridge ones for instance.

Using the three adsorption complexes shown in Fig. 2 and a 4×4 surface supercell, the SuSMoST toolkit generated 261 distinct configurations, each with two molecules per cell. To limit the number of configurations, we set a maximum cut-off radius of 5 Angstroms between molecules. From these parameters, the program created high-coverage systems comprising various overlayer arrangements, including top/top, top/bridge, and bridge/bridge combinations. We further filtered configurations by considering only realistic lateral interactions, achieved through the hard-sphere potential of lateral interactions as implemented in SuSMoST using the following hard sphere radii for the chemical elements of the adsorbate: $S = 1.5$ $C = 1.2$ N $= 1.2$ $H = 0.5$ and $O = 1.3$ $\dot{A}$. Consequently, configurations with infinite interaction energy between the two adsorbed molecules were discarded. Following these

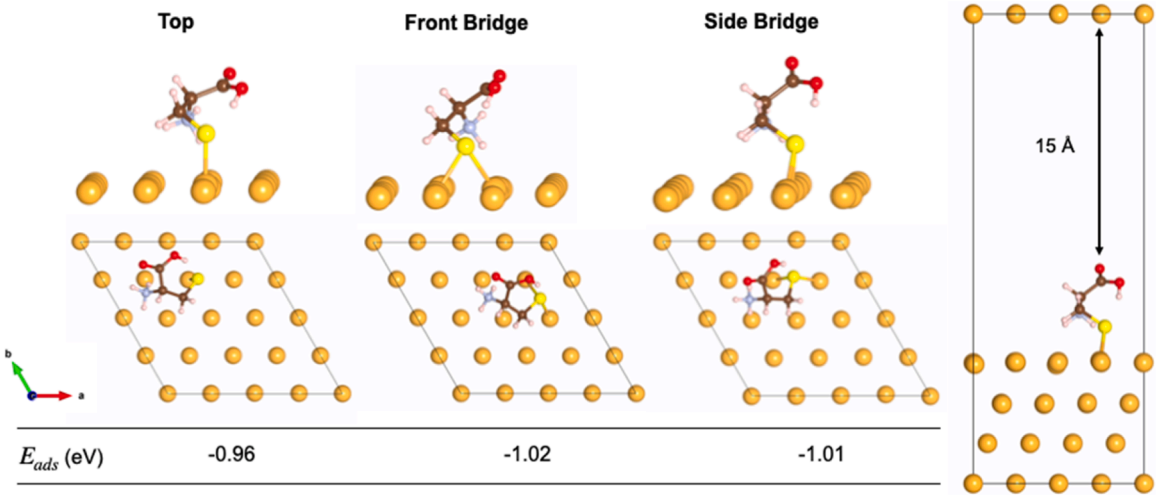

Fig. 2. Set of adsorption complexes used in this work to sample the lattice model at high coverage. Legend: Au = orange, S = yellow, O = red, N = blue, C = brown, and H = white.

selection steps, we obtained 30 different configurations. All the final configurations were carefully analyzed, and the 16 configurations presented in this work were selected based on our objective to investigate the impact of adsorption sites, inter-molecular interactions, and overall surface organization on the system's global stability.

All the slab models investigated in this study are provided in Figure SI.1 of the Supplementary Information. Fig. 3 showcases four representative configurations to give an overview of the different arrangements explored. Fig. 4 illustrates the principal interactions that are characteristic of all the selected configurations, highlighting the diversity and complexity of these interactions. For clarity, the systems are designated based on their adsorption sites: TT for top/top, TB for top/bridge, and BB for bridge/bridge.

An interesting observation is the variations in the global surface arrangement. Notably, we found a dominance of TT and TB configurations compared to BB. For all configurations, inter-molecular interactions primarily occur through the formation of hydrogen bonds between the carbonyl group of one cysteine and the charged amino group of another. Intra-molecular interactions were also observed in some systems, where a hydrogen bond forms within the same molecule. Configurations without interactions between organic molecules, such as those seen in surface arrangements TB3, TT4, and TT7 (see Figure SI.1), were also considered. Finally, to validate our methodology, it is important to note that the program was able to find a known geometry previously described by Morales-Vidal et al. [22] (system TT2).

4. Results and discussion

4.1. Energetic analysis

In this study, we examined three types of energies. Firstly, we assessed the adsorption energy per molecule, calculated according to Eq. (1).

$$E_{ads} = (E_{S-L} - E_S - nE_L)/n \quad (1)$$

Where E_{S_L} is the total energy of the optimized system containing the ligand on the metallic surface, E_S is the total energy of the optimized gold surface, E_L is the total energy of one ligand from the optimized gas structure and n is the number of molecules adsorbed per cell.

Secondly, we analyzed the adsorption energy of the overlayer (Adhesion energy, E_{adh}), wherein instead of considering only one cysteine molecule in Eq. (1) as E_L, we assessed the energy of the complete periodic organic overlayer using a single-point energy calculation. The periodic organic overlayer refers to the repeating arrangement of cysteine molecules adsorbed onto the surface, which is obtained by manually removing the gold atoms from the full system, leaving only the organic layer for analysis.

$$E_{adh} = E_{S-L} - E_S - E_{Overlayer} \quad (2)$$

Lastly, we calculated the interaction energy E_{int} of every configuration using Eq. (3), which quantifies the interaction between two molecules on the surface. All acronyms used to define the energies E_S, E_L, E_{S_L}, E_{S-L_1}, E_{S-L_2} and $E_{Overlayer}$ are illustrated in Figure SI.2 for clarity.

$$E_{int} = E_{S-L} - E_{S-L_1} - E_{S-L_2} + E_S \quad (3)$$

All computed energies and the charge analysis are summarized in Table 1. Note that some of the configurations were rearranged after DFT optimization. The initial (in parentheses) and final arrangements are given in Table 1 and an example of such reorganization is shown in Figure SI.3 with the system TB6. Overall, all configurations have total energies that are quite close, with a difference of 1.078 eV between the most (TB7) and least (TT7) stable configurations. When evaluating the adsorption energy using Eq. (1), the results range from −0.904 eV (system TT7) to −1.443 eV (system TB7), showing a maximum difference of only 0.539 eV between the selected configurations. Curiously, using Eq. (2) to evaluate the adhesion energy of the overlayer, we observe the opposite trend, with configuration TT7 being the most stable and TB7 the least stable. Additionally, we observe that the combination of adsorption sites has no significant impact on the stability of the different systems. This indicates that the stabilization of the system is not directly related to how the cysteine molecule is adsorbed on the

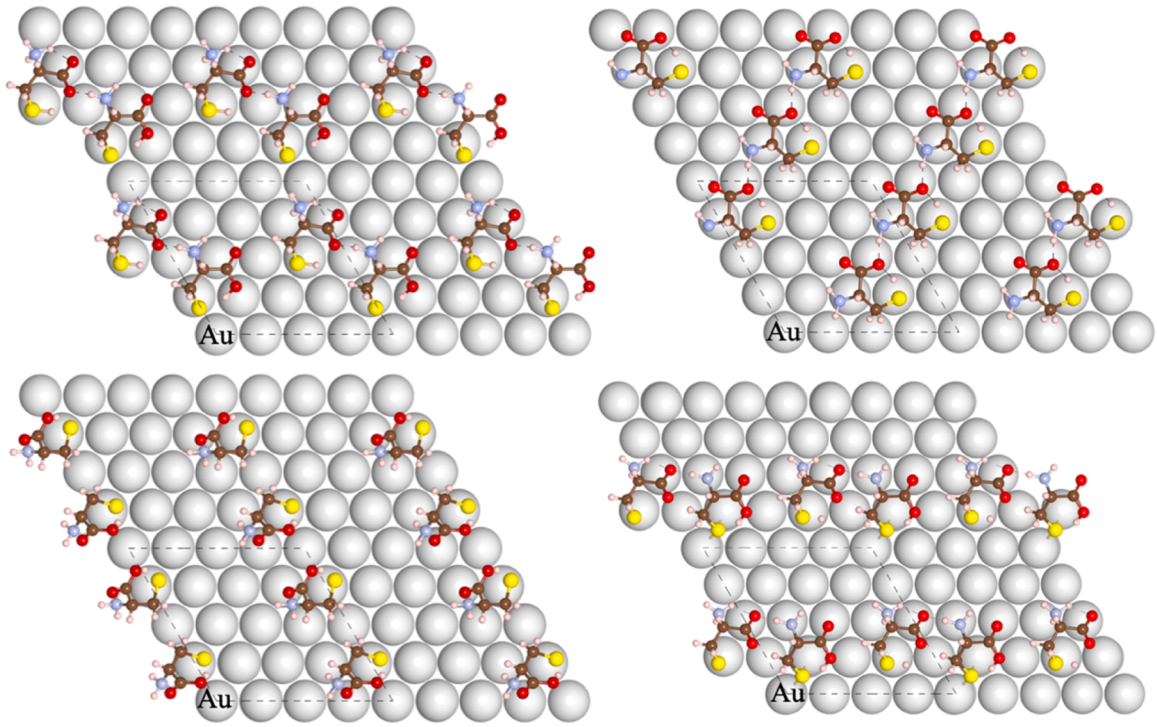

Fig. 3. Examples of selected surface samples obtained with pairs of adsorption complexes. Top left: system TT2; Top right: system TT5; Bottom left: system TT7; Bottom right: system TB7.

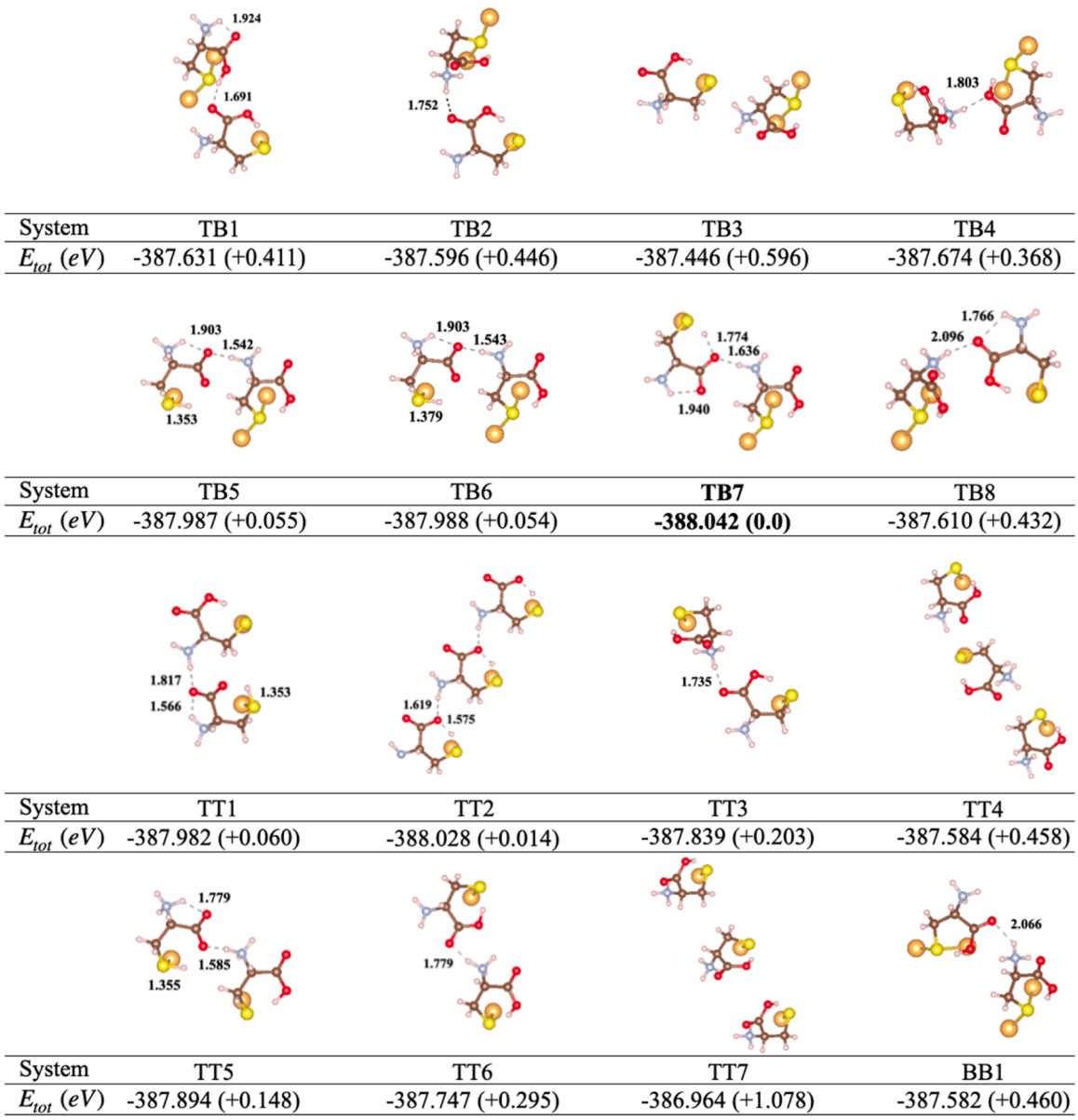

System	TB1	TB2	TB3	TB4
E_{tot} (eV)	-387.631 (+0.411)	-387.596 (+0.446)	-387.446 (+0.596)	-387.674 (+0.368)

System	TB5	TB6	**TB7**	TB8
E_{tot} (eV)	-387.987 (+0.055)	-387.988 (+0.054)	**-388.042 (0.0)**	-387.610 (+0.432)

System	TT1	TT2	TT3	TT4
E_{tot} (eV)	-387.982 (+0.060)	-388.028 (+0.014)	-387.839 (+0.203)	-387.584 (+0.458)

System	TT5	TT6	TT7	BB1
E_{tot} (eV)	-387.894 (+0.148)	-387.747 (+0.295)	-386.964 (+1.078)	-387.582 (+0.460)

Fig. 4. Set of optimized overlayer structures for all selected configurations. Distances are given in Angstrom and the total and relative energies (in parentheses) of the periodic systems are expressed in eV. The most stable system is highlighted in bold and serves as a reference for the relative energies.

surface, but rather to the type of interactions present within the organic overlayer. Regarding the interaction energy, stabilizing interactions are observed for all systems except TT7, which has a positive interaction energy of 0.139 eV.

This study revealed a close relationship between the interaction energy and the adsorption energy calculated per molecule. Fig. 5a displays the adsorption energy computed using Eq. (1) as a function of the interaction energy. It illustrates a strong linear correlation between the two quantities ($r^2 = 0.91$) and three distinct groups are apparent. However, as already mentioned, despite the apparent grouping of stabilization effects, it bears no relation to how cysteine molecules are adsorbed on the surface.

Configuration TT7 being the only one representative of a surface arrangement where no inter-molecular interactions are present leads to less stable adsorption energy. The common factor among the most stable configurations (with E_{ads} ranging from −1.443 to −1.369 eV) is the formation of an SH bond after geometry optimization, which introduces intramolecular interactions. These results suggest that this specific structural arrangement enhances the adsorption of cysteine on the gold surface.

Furthermore, the equation representative of this linear correlation tells us that for every increase of the interaction energy, the adsorption energy will be increased by 25 %. It is noticeable that when the interaction energy goes to zero, meaning no interaction, identical to a low-coverage system, the adsorption energy is −1.03 eV according to the equation $y = 0.25x - 1.03$. This value is very close to the energy value found in the bridge low-coverage systems used as adsorption complexes (−1.02 and −1.01 eV), confirming the absence of lateral interactions in low-coverage systems. By utilizing the SuSMoST toolkit, we discovered the previously identified configuration, defined as TT2. However, our work revealed a new and slightly more stable configuration, referred to as TB7, as depicted in Fig. 4. The TB7 system demonstrates a slightly higher stability in adsorption energy (−1.443 eV) compared to the configuration reported in the literature TT2 (−1.436 eV). Although the difference is minimal, it suggests that exploring diverse configurations may lead to the discovery of more stable systems. The TT2 system was deemed highly stable due to the presence of inter-molecular hydrogen bonds between [NH_3^+] and [COO^-] moieties, akin to those observed in

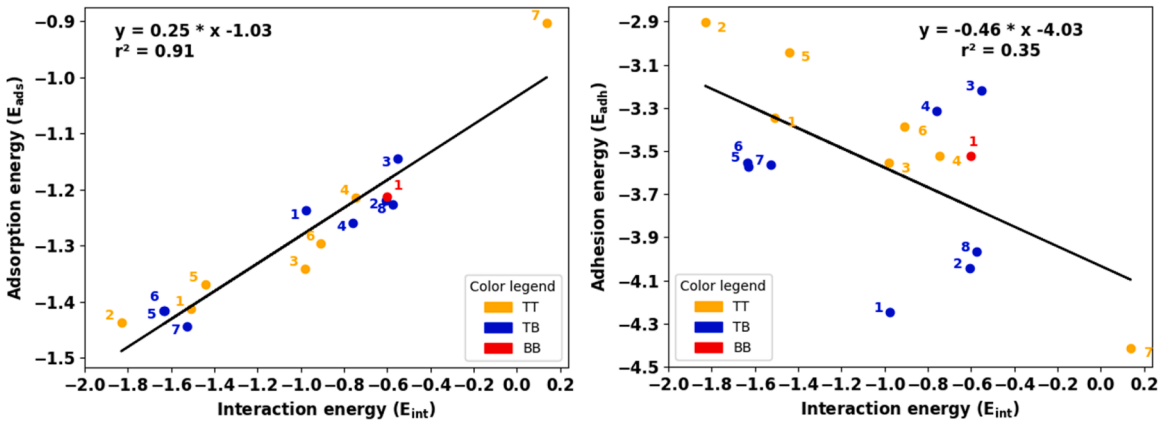

Fig. 5. (a) Adsorption energy (E_{ads}) as a function of the interaction energy (E_{int}). (b) Adhesion energy (E_{adh}) as a function of the interaction energy (E_{int}). All energies are given in eV.

the crystal structure of l-cysteine with an H-bond of 1.6 $\dot{A}$. However, despite the TB7 system also displaying a hydrogen bond with a distance of approximately 1.6 $\dot{A}$, it additionally showcases an intra-molecular interaction between the charged amino group and the carboxylic group of the same molecule, increasing its stability. Configurations TB5 and TB6 are found to be similar after DFT relaxation although their initial geometry was different as one can see in Table 1. They show similar total energy but a slight change in the geometry of the overlayer is enough to create differences when computing the adsorption energy of the overlayer or the interaction energy as an example (E_{int}: −1.636 vs −1.628 eV).

In Fig. 5b, we examine the adsorption strength of the overlayer using Eq. (2). Using that methodology, we disregard the interaction of individual cysteine molecules with the surface but we consider the interaction of the entire organic overlayer already engaged. In this scenario, no linear correlation between the two quantities is evident ($r^2 = 0.35$). Specifically, we observe that the weaker the stabilizing effect of the interaction, the greater the stabilization of the overlayer's adsorption energy. In addition, we do not observe any group of stabilization as compared to Fig. 5a. The tendency is even opposite, indicating that as the overlayer becomes more stable, its interaction with the gold surface becomes less favorable. A more stable overlayer is less likely to benefit from interactions with the surface. This shows that the stabilization of the overlayer is crucial to have a stable system but it can also hinder proper adhesion to the surface.

Comparing the adsorption and the adhesion energies yields valuable insights. A more negative E_{adh} compared to the E_{ads} indicates that intermolecular interaction outweighs the interaction of the organic layer with the metallic surface. Conversely, suppose the adsorption energy per molecule is more negative than that calculated considering the overlayer. In that case, it suggests that the presence of multiple molecules on the surface in interaction stabilizes the configuration in which the molecule is adsorbed into the surface. These results suggest that an equilibrium between the stabilization of the overall arrangement and the interaction of the organic molecules with the surface is quite sensitive to the type of interactions.

4.2. Electronic structure analysis

To gain more insight we examined the Bader charges of each atom and more specifically of the sulfur atoms. The charges found on the sulfur atoms for the low-coverage systems, i.e., the adsorption complexes depicted in Fig. 2, were of −0.254 |e| and −0.263 |e| for the bridge and the top sites respectively. As indicated in Table 1, the Bader charges on the sulfur atoms bonded to the surface either align with the charges observed for the corresponding low-coverage adsorption complexes or exhibit a charge near zero or positive. We observed differences in the charge on the sulfur atoms in configurations where intramolecular interactions occurred between the $[NH_3^+]$ and [COOH] groups of the same cysteine molecule. These interactions were consistently present only in the molecules positioned on the top site. Consequently, the variation in charge from low-coverage representation was observed exclusively in the sulfur atom at the top site. However, in the case of configuration TT2, where all cysteines occupied the same site, sulfur atom charges matched perfectly as the global overlayer geometry is symmetrical. This phenomenon can be explained by the fact that the shift in electronic density due to intra-molecular interaction caused sulfur to lose electron density, resulting in reduced transfer to gold. This effect arises from the displacement of the hydrogen from the carboxylic group towards sulfur, diminishing its nucleophilic character.

We found that the most stable systems are those with notable charges on one of the sulfur atoms. In these systems, the charge transfer from the molecule to the surface is also affected. Specifically, the charge transfer from the overlayer to the metallic surface decreases when one of the sulfur atoms becomes positively charged, indicating a reduction in the electron density available for transfer.

Fig. 6 highlights the charge density (Fig. 6a) and the charge density difference (Figs. 6b and 6c) of the system TT1. This configuration is interesting as it features two sulfur atoms bonded to the surface on a top position but where the sulfur atoms present different charges and opposite in sign. This behavior is also observed in configurations TB5, TB6, and TT5. In all cases, the charge density difference around the two sulfur atoms is distinct: the isosurface area of charge depletion around S1 is more spread out than around S2 (or inverse). At first glance, in the example of system TT1, this result seems counterintuitive, as we would expect more charge loss on S2 since it carries the positive charge (see Fig. 6c). However, before adsorption onto the surface and the creation of the S-Au bond, we observed a charge of −0.617 |e| for S1 and −0.083 |e| for S2. The overall organization of the overlayer led to a modification of the electronic density and, consequently, changes in the charges carried by the sulfur atoms. In the case of configuration TT1, this is explained by the creation of the SH bond, which has shifted the electronic density of the sulfur atom towards the bond. As a result, the charge loss on S1 is more significant than on S2, explaining the resulting charges observed. These results are observed for all systems presenting a difference in sign on the sulfur atoms.

In addition, the adsorption of the molecule caused a redistribution of electrons within the top surface layer, leading to a gain of charge on top of the surface (see Fig. 6b). This result is confirmed by the positive charge transfer of 0.418 |e| from the organic overlayer to the metallic

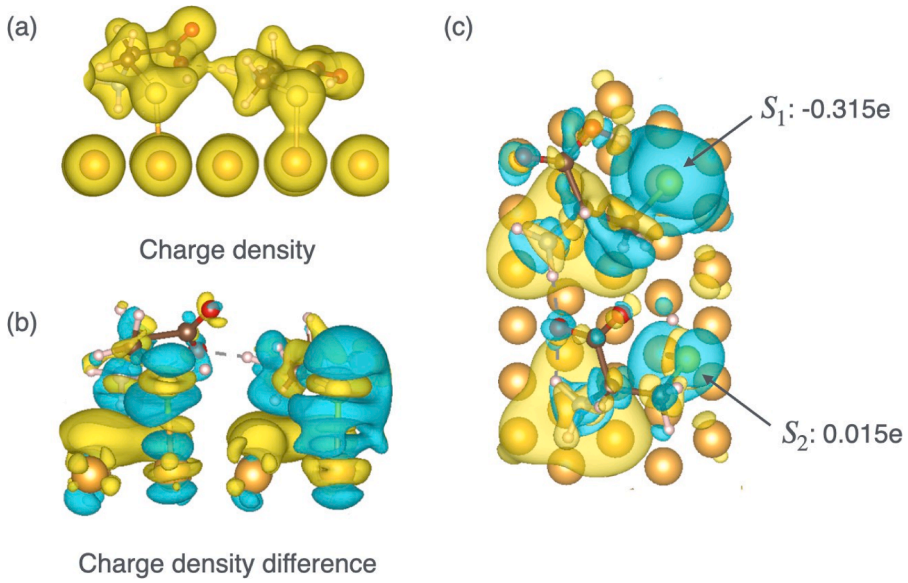

Fig. 6. Isosurface representation of charge density and charge density difference for the system TT1. (a) Charge density distribution. (b) Side view of the charge density isosurface. (c) Top view of the charge density isosurface. Yellow regions indicate charge gain, while blue regions indicate charge depletion. The isosurface level is set at 0.001 e/Å^3.

surface as calculated for this system.

5. Conclusions

This study shows that automated sampling of adsorption mono-layer configurations with designated tools, such as SuSMoST, is a necessary part of the robust methodology of future SAM studies. Our investigation into the surface interactions of the deprotonated acidic form of L-cysteine with the gold (111) surface at high coverage yields significant insights. Through extensive computational analyses and DFT optimizations, we examined various adsorption configurations and their implications for stability and charge distribution within the organic overlayer. Our findings indicate that, at high ligand coverage, the energetic analyses reveal distinct correlations, underscoring the predominance of intra-layer interactions over surface site arrangements in determining overall stability. Bader charge analysis further highlights the critical role of charge distribution at sulfur atoms, particularly in configurations characterized by intra-molecular interactions. Notably, our exploration of overlayer adsorption energies uncovers a complex relationship between interaction strengths and stability, suggesting that more stable overlayers may paradoxically exhibit weaker interactions with the underlying surface. This study introduces a novel methodology for automatically generating high-coverage configurations using the SuSMoST toolkit, providing a robust framework for future research in this area.

CRediT authorship contribution statement

Mary Tabut: Writing – original draft, Methodology, Formal analysis. **Pavel V. Stishenko:** Writing – original draft, Software. **Monica Calatayud:** Writing – original draft, Conceptualization.

Declaration of competing interest

The authors declare the following financial interests/personal relationships which may be considered as potential competing interests:

Monica Calatayud reports financial support was provided by Sorbonne University. Monica Calatayud reports a relationship with Sorbonne University that includes: employment. If there are other authors, they declare that they have no known competing financial interests or personal relationships that could have appeared to influence the work reported in this paper.

Acknowledgement

This research received partial funding from the French National Research Agency (ANR) through the project ANR-22-CE09–0007–01. We gratefully acknowledge financial support from the Initiative Sciences et Ingénierie Moléculaires (iSiM) at Sorbonne Université. This work was performed using HPC resources from GENCI-IDRIS Grant 2023-A0150802131.

Supplementary materials

Supplementary material associated with this article can be found, in the online version, at doi:10.1016/j.susc.2025.122740.

Data availability

Data will be made available on request.

References

[1] C. Love, L.A. Estroff, J.K. Kriebel, R.G. Nuzzo, G.M. Whitesides, Self-assembled monolayers of thiolates on metals as a form of nanotechnology, Chem. Rev. 105 (4) (2005) 1103–1170.
[2] R. Bhure, A. Mahapatro, Surface patterning using self assembled monolayers (sams), Biomaterials (2010) 65–107.
[3] C. Vericat, M.E. Vela, G. Corthey, P. E, E. Cortés, M.H. Fonticelli, F. Ibañez, G. E. Benitez, P. Carro, R.C. Salvarezza, Self-assembled mono-layers of thiolates on metals: a review article on sulfur-metal chemistry and surface structures, in: RSC. Adv., 4, 2014, pp. 27730–27754.
[4] J. Gooding, F. Mearns, W. Yang, J. Liu, Self-assembled monolayers into the 21st century: recent advances and applications, Int. J. Devot. Fundamen. Practic. Aspects Electroanaly. 15 (2) (2003) 81–96.
[5] D. Costa, C.M. Pradier, F. Tielens, L. Savio, Adsorption and self-assembly of bio-organic molecules at model surfaces: a route towards increased complexity, Surf. Sci. Rep. 70 (4) (2015) 449–553.
[6] M. Prato, R. Moroni, F. Bisio, R. Rolandi, L. Mattera, O. Cavalleri, M. Canepa, Optical characterization of thiolate self-assembled monolayers on au (111), J. Physic. Chem. C 112 (10) (2008) 3899–3906.
[7] M. Singh, N. Kaur, E. Comini, The role of self-assembled monolayers in electronic devices, J. Mater. Chem. C 8 (12) (2020) 3938–3955.
[8] R. Yi, Y. Mao, Y. Shen, L. Chen, Self-assembled monolayers for batteries, J. Am. Chem. Soc. 143 (33) (2021) 12897–12912.

[9] Z. Weng, F. Zaera, Increase in activity and selectivity in catalysis via surface modification with self-assembled monolayers, J. Physic. Chem. C 118 (7) (2014) 3672–3679.
[10] D.B. Amabilino, Chirality At the nanoscale: nanoparticles, surfaces, Materials and More, John Wiley & Sons, 2009.
[11] E. Longo, A. Orlandin, F. Mancin, P. Scrimin, A. Moretto, Reversible chirality control in peptide-functionalized gold nanoparticles, ACS. Nano. 7 (11) (2013) 9933–9939.
[12] E. Severoni, S. Maniappan, L.M. Liz-Marzan, J. Kumar, F.J. Garcia de Abajo, L. Galantini, Plasmon-enhanced optical chirality through hotspot formation in surfactant-directed self-assembly of gold nanorods, ACS. Nano. 14 (12) (2020) 16712–16722.
[13] D. Karhanek, Self-assembled monolayers studied by density-functional theory, na (2010).
[14] M.J. Ford, R.C. Hoft, A. McDonagh, Theoretical study of ethynylbenzene adsorption on au (111) and implications for a new class of self-assembled monolayer, J. Physic. Chem. B 109 (43) (2005) 20387–20392.
[15] E. Boz, M. Stein, Accurate receptor-ligand binding free energies from fast qm conformational chemical space sampling, Int. J. Mol. Sci. 22 (6) (2021) 3078.
[16] J.M. McMahon, Ground-state structures of ice at high pressures from ab initio random structure searching, Physic. Rev. B—Cond. Matter Mater. Phys. 84 (22) (2011) 220104.
[17] C.J. Pickard, R.J. Needs, Ab initio random structure searching, J. Phys. 23 (5) (2011) 053201.
[18] J. Zhang, Q. Chi, J.U. Nielsen, E.P. Friis, J. Andersen, J. Ulstrup, Two-dimensional cysteine and cystine cluster networks on au (111) disclosed by voltammetry and in situ scanning tunneling microscopy, Langmuir. 16 (18) (2000) 7229–7237.
[19] R. Di Felice, A. Selloni, Adsorption modes of cysteine on au (111): thiolate, amino-thiolate, disulfide, J. Chem. Phys. 120 (10) (2004) 4906–4914.
[20] J. Fajin, J. Gomes, M.N. Cordeiro, Dft study of the adsorption of D-(l-) cysteine on flat and chiral stepped gold surfaces, Langmuir. 29 (28) (2013) 8856–8864.
[21] R. Di Felice, A. Selloni, E. Molinari, Dft study of cysteine adsorption on au (111), J. Physic. Chem. B 107 (5) (2003) 1151–1156.
[22] J. Morales-Vidal, N. Lopez, M.A. Ortuno, Chirality transfer in gold nanoparticles by L-cysteine amino acid: a first-principles study, J. Physic. Chem. C 123 (22) (2019) 13758–13764.
[23] A. His, B. Liedberg, Chemisorption of L-cysteine and 3-mercaptopropionic acid on gold and copper surfaces: an infrared reflection-absorption study, J. Colloid. Interface Sci. 144 (1) (1991) 282–292.
[24] N. Khalfaoui-Hassani, M. Tabut, N.H. Awe, C. Desmarets, D. Toffoli, M. Stener, N. Goubet, M. Calatayud, C. Salzemann, The intriguing role of L-cysteine in the modulation of chiroplasmonic properties of chiral gold nano-arrows, Nanoscale (2025).
[25] S. Yau, C.J. Huang, W. Liao, Stm characterization of self-assembled mono-layers of cysteine betaine on au (111) electrode in perchloric and sulfuric acids, J. Physic. Chem. C 121 (31) (2017) 16845–16853.
[26] S. Akimenko, G. Anisimova, A. Fadeeva, V. Fefelov, V. Gorbunov, T. Kayumova, A. Myshlyavtsev, M. Myshlyavtseva, P.V. Stishenko, Susmost: surface science modeling and simulation toolkit, J. Comput. Chem. 41 (23) (2020) 2084–2097.
[27] G. Kresse, J. Furthmüller, Efficiency of ab-initio total energy calculations for metals and semiconductors using a plane-wave basis set, Comput. Mater. Sci. 6 (1) (1996) 15–50.
[28] G. Kresse, J. Furthmüller, Efficient iterative schemes for ab initio total-energy calculations using a plane-wave basis set, Physic. Rev. B 54 (16) (1996) 11169.
[29] G. Kresse, J. Furthmüller, Efficient iterative schemes for ab initio total-energy calculations using a plane-wave basis set, Physic. Rev. B 54 (16) (1996) 11169.
[30] P.E. Bloch, Projector augmented-wave method, Physic. Rev. B 50 (24) (1994) 17953.
[31] J.P. Perdew, K. Burke, M. Ernzerhof, Generalized gradient approximation made simple, Phys. Rev. Lett. 77 (18) (1996) 3865.
[32] M. Rosa, S. Corni, R. Di Felice, van der waals effects at molecule-metal interfaces, Physic. Rev. B 90 (12) (2014) 125448.
[33] S. Grimme, J. Antony, S. Ehrlich, H. Krieg, A consistent and accurate ab initio parametrization of density functional dispersion correction (dft-d) for the 94 elements h-pu, J. Chem. Phys. 132 (15) (2010) 154104.
[34] H.J. Monkhorst, J.D. Pack, Special points for brillouin-zone integrations, Physic. Rev. B 13 (12) (1976) 5188.
[35] G. Henkelman, A. Arnaldsson, H. Jónsson, A fast and robust algorithm for bader decomposition of charge density, Comput. Mater. Sci. 36 (3) (2006) 354–360.
[36] E. Sanville, S.D. Kenny, R. Smith, G. Henkelman, Improved grid-based algorithm for bader charge allocation, J. Comput. Chem. 28 (5) (2007) 899–908.
[37] W. Tang, E. Sanville, G. Henkelman, A grid-based bader analysis algorithm without lattice bias, J. Phys. 21 (8) (2009) 084204.
[38] H. Gharabekyan, J. Koetz, A.H. Poghosyan, A protonated L-cysteine adsorption on gold surface, Int. J. Devoted Princ. Appl. Colloid Interface Sci. 629 (2021).